MoS_2 flakes stabilized with DNA/RNA nucleotides: *In vitro* cell response

M. Cicuéndez[a,b,*,+], V. S. Silva[c,*,+], J. Santos[c], A. Coimbra[c], H. Oliveira[a,c], M. Ayán–Varela[d], J. I. Paredes[d], S. Villar–Rodil[d], M. Vila[b]

[a]CICECO- Aveiro Institute of Materials, Chemistry Department. University of Aveiro (UA). Campus Universitário de Santiago. 3810-193 Aveiro, Portugal.

[b]NRG-TEMA, Mechanical Engineering Department. University of Aveiro (UA). Campus Universitário de Santiago. 3810-193 Aveiro, Portugal.

[c]CESAM & Department of Biology. University of Aveiro. Campus Universitário de Santiago, 3810-193 Aveiro, Portugal.

[d]Instituto Nacional del Carbón, INCAR-CSIC, C/Francisco Pintado Fe 26, 33011 Oviedo, Spain.

***Corresponding author**:
E-mail address: monicacicuendez@hotmail.com (Mónica Cicuéndez); vsilsa@ua.pt (Virgília Silva)

[+]these authors contributed equally to this work.

ABSTRACT

Two-dimensional transition metal dichalcogenides (TMDCs), such as MoS_2 and WS_2, have recently emerged as nanomaterials with potential use in biomedicine. An attractive means to favor their interaction with biological media is the use of proper biomolecules as exfoliating/dispersing agents. Here, MoS_2 flakes were stabilized with different small functional biomolecules such as adenosine monophosphate (AMP), guanosine monophosphate (GMP) and flavin mononucleotide (FMN) through the strong nucleotide−MoS_2 interaction of Lewis acid-base type, rather than just on the weak dispersive and hydrophobic forces commonly associated with the use of many surfactants. The impact of the nucleotide-stabilized MoS_2 flakes on the viability and cell proliferation, on the production of intracellular reactive oxygen species (ROS), and on the preosteoblast differentiation process (early stage) has been also evaluated, as well as the incorporation and intracellular localization of the nanomaterials by MC3T3-E1 and Saos-2 cells. The nucleotide-stabilized MoS_2 flakes were found to exhibit excellent biocompatibility. Furthermore, their incorporation did not affect the integrity of the cell plasma membrane, which makes them ideal candidates for delivering drug/gene directly into cells. The *in vitro* cell response of tumor cells to these nanomaterials differs from that of undifferentiated cells, which provides the basis for their potential use in cancer therapy.

Keywords: transition metal dichalcogenides (TMDCs), MoS_2, biodispersants, biocompatibility, *in vitro* cell response, osteoblast.

1. INTRODUCTION

A new class of two-dimensional (2D) nanomaterials, transition metal dichalcogenides (TMDCs) such as MoS_2, $MoSe_2$, WS_2, and WSe_2, which possess a wide array of useful properties, has recently drawn attention for a variety of biomedical applications [1-10] including their use as drug delivery agents, therapeutic, or bio-imaging agents, as well as biosensors. However, some issues must be addressed for their actual implementation as biomaterials. Indeed, 2D TMDCs, being rather hydrophobic materials, do not generally form stable colloidal dispersions in water and aqueous biological media by themselves, which makes their *in vivo* applications difficult [11]. Moreover, TMDCs are not intrinsically biocompatible and usually require functionalization for their incorporation into biological systems [12]. Both issues can be simultaneously addressed by the use of appropriate dispersants. Indeed, TMDC aqueous dispersions can be prepared with the assistance of stabilizers of amphiphilic nature. Although a number of synthetic dispersants have been successfully used toward the exfoliation and stabilization of TMDCs in aqueous dispersion [13,14], that at the same time have also provided biocompatibility [15] (e.g., polyethyleneglycol [16]) innocuous, non-toxic stabilizers of natural origin are potentially the most appropriate choice from the perspective of biomedical applications. Indeed, the use of stabilizers of natural origin (*i.e.*, biomolecule-based dispersants) such as proteins [17] or DNA [18] offers potential advantages associated with an improved biocompatibility of the 2D nanomaterials. Moreover, the smaller physical dimensions of these natural stabilizers compared to those of polymers, would render the cellular uptake process easier for different biomedical purposes such as cell labeling and drug/gene delivery directly into cells. In this context, our research group has recently proposed several nucleotides as efficient exfoliating/dispersants agents of TMDCs in aqueous medium [19]. Indeed, we have

reported a novel stabilization mechanism, which relies on a specific, relatively strong nucleotide−TMDC interaction of Lewis acid-base type, rather than just on the weak dispersive and hydrophobic forces commonly associated with the use of many surfactants. In our previous report, a preliminary biocompatibility study in the presence of nucleotide-stabilized MoS_2 flakes suggested their prospective use in biomedicine. Here, we provide an in-depth study on the biocompatibility of MoS_2 flakes stabilized with adenosine monophosphate (AMP), guanosine monophosphate (GMP) and flavin mononucleotide (FMN). Specifically, a comparative study of the cellular response of MC3T3-E1 preosteoblasts as undifferentiated cells and Saos-2 human sarcoma osteoblasts exposed to different concentrations of nucleotide-stabilized MoS_2 flakes has been carried out, evaluating their impact on the viability and cell proliferation, cellular incorporation process, reactive oxygen species production and preosteoblast differentiation process (early stage). The obtained results highlight that nucleotide-stabilized MoS_2 flakes can be proposed as candidates for photothermal therapy, and as nano-vehicles for the transport of therapeutic agents at the sub-cellular level.

2. MATERIALS AND METHODS

2.1. Preparation of colloidal dispersions of MoS_2 in water assisted by nucleotides

MoS_2 powder and the nucleotides AMP, GMP, and FMN were obtained from Sigma-Aldrich and used as received. MoS_2 in powder form was added to an aqueous solution of a given nucleotide (AMP, GMP or FMN; 1 mg mL^{-1}) at a MoS_2/nucleotide mass ratio of 30:1, and then the mixture was sonicated in an ultrasound bath cleaner for 5 h (J.P. Selecta Ultrasons system; frequency: 40 kHz; power: ~20 W L^{-1}). The resulting sonicated suspension was centrifuged at 200g for 20 min (Eppendorf 5424 microcentrifuge) to sediment poorly exfoliated or non-exfoliated particles and the top

~75% of the supernatant volume was collected for subsequent use. To remove the free, non–adsorbed nucleotide molecules from the resulting dispersion, it was typically subjected to two iterative cycles of sedimentation via centrifugation (20000 g, 20 min), replacement of two thirds of the resulting supernatant solution by milli–Q water and re-dispersion of the sedimented flakes in this new solution by a brief (2 min) sonication step.The final MoS_2 dispersions stabilized with AMP, GMP or FMN nucleotides are subsequently referred to in the text as MoS_2–AMP, MoS_2–GMP and MoS_2–FMN, respectively. The concentration of the MoS_2 dispersions was estimated from the extinction value at the local minimum of ≈345 nm using a calculated extinction coefficient of e≈6900 L g^{-1} m^{-1} [20].

2.2. Characterization of the MoS_2 dispersions

The exfoliated MoS_2 materials were characterized by UV–vis absorption (extinction) spectroscopy, X-ray photoelectron spectroscopy (XPS), Raman spectroscopy and scanning transmission electron microscopy (STEM). UV–vis absorption/extinction spectra were recorded on a double-beam Helios spectrophotometer (Thermo Spectronic) with an optical path length of 1 cm. XPS was carried out on a SPECS apparatus working at a pressure of 10^{-7} Pa with a non-monochromatic Mg K_α X-ray source (1253.6 eV) operated at 11.81 kV and 100 W. Raman spectra were obtained with a Horiba Jobin–YvonLabRam instrument at a laser excitation wavelength of 532 nm and an incident laser power of 0.5 mW. Samples for XPS and Raman spectroscopy were prepared by drop–casting the aqueous MoS_2 dispersions onto pre-heated metallic sample holders until uniform films covered the substrate and allowing them to dry under ambient conditions. STEM imaging was performed on a Quanta FEG 650 system (FEI Company) operated at 20–25kV. Specimens for this technique were prepared by mixing

isopropanol and an aqueous MoS_2 dispersion in 1:2 volume ratio. Subsequently, ~20 μL of the mixed suspension were drop-cast onto a copper grid (200 mesh) covered with a continuous carbon film (Electron Microscopy Sciences) and allowed to dry under ambient conditions.

2.3. Viability and cellular proliferation

MC3T3-E1 preosteoblasts, as undifferentiated osteoblast-like cells (mouse C57BL/6 calvaria) and human Saos-2 osteoblasts, as an osteosarcoma cell line, were seeded with a cell density of 1×10^5 cells mL^{-1} in Minimum Essential Medium (MEM) Alpha modifications (Sigma-Aldrich) and Dulbecco's Modified Eagle Medium (DMEM, Sigma-Aldrich), respectively, supplemented with 10% fetal bovine serum (FBS, Gibco BRL), 1 mM L-glutamine (Sigma-Aldrich), penicillin (800 μg mL^{-1}, BioWhittaker Europe) and streptomycin (800 μg mL^{-1}, BioWhittaker Europe) under CO_2 (5%) in humidified atmosphere at 37ºC for 24 h. Then, the culture medium was replaced by a fresh one with nucleotide-stabilized MoS_2 final concentrations of 10–75 μg mL^{-1} (with 5 min of bath sonication to homogenize the mixture) and the cell culture was exposed to the nanomaterials for 24 h. After the incubation period, the cells were washed with phosphate-buffered saline (PBS, Sigma-Aldrich) to remove the non-incorporated nanomaterials and incubated with 0.25% trypsin-EDTA (0.25% trypsin, 1 mM EDTA) (Biochrom). Control samples corresponding to cells cultured in the absence of MoS_2 were included in all the assays. Trypan blue dye exclusion test was used for the quantitative evaluation of viability and cell proliferation. All the cells that exclude the dye are considered viable, as it selectively stains dead cells or cells with damaged cell membranes. Cell counting was performed using a hemocytometer (Neubauer chamber).

2.4. Cellular incorporation of MoS_2 flakes

The incorporation of MoS_2 stabilized with different mononucleotides (AMP, GMP and FMN) by MC3T3-E1 and Saos-2 cells was evaluated by light scattering flow cytometry [21], which is a simple method to evaluate the potential of incorporation of nanomaterials by mammalian cells [22]. In flow cytometry, light scattering at 90° dispersion angle is called side–scatter light (SSC), determined in part by the cellular cytoplasm, mitochondria, and pinocytic vesicles [23], its intensity being proportional to the intracellular complexity. Laser light that is collected at small angles is called the forward–scatter light (FSC), its intensity being proportional to the size of the cell. These intrinsic cellular parameters allow verifying the incorporation of any nanomaterial by diverse mammalian cell types [22]. The SSC and FSC parameters were measured on a Coulter XL (Beckman Coulter, Hialeah, FL-USA) flow cytometer equipped with an argon laser (15 mW, 488 nm). The data were acquired using the System II v. 3.0 (Beckman Coulter, Hialeah, FL). For each sample, 5000–20000 cells were analyzed with a flow of 1000 cells s^{-1}. MC3T3-E1 pre-osteoblasts and human Saos-2 osteoblasts were seeded with a cell density of 1×10^5 cells mL^{-1} in MEM and DMEM medium, respectively, supplemented as described above. Subsequently, the culture medium was replaced by a fresh one containing nanomaterials at final concentrations of 10 and 50 μg mL^{-1} (with 5 min of bath sonication to homogenize the mixture) and the cells were incubated at 37ºC with such nanomaterial concentrations for either 4 h or 24 h. To study temperature-related inhibition of endocytosis, the same experiments were performed at 4ºC [21]. After the exposure period, the cells were repeatedly washed with PBS, incubated with 0.25% trypsin-EDTA and re–suspended in fresh supplemented culture medium for analysis by flow cytometry. Control samples corresponding to cells cultured in the absence of MoS_2 were included in all the assays.

2.5. Intracellular reactive oxygen species production

To evaluate the intracellular reactive oxygen species (ROS) production, MC3T3-E1 pre-osteoblasts and human Saos-2 osteoblasts were similarly seeded with a cell density of 1×10^5 cells mL^{-1} for 24 h as described above. Again, after the incubation time, the culture medium was replaced by a fresh one containing 10 and 50 μg mL^{-1} of the nanomaterials and the cell culture was incubated for 24 h. After the exposure period, the cell culture was washed with PBS and incubated with 10 μM of the 2',7'-dichlorodihydro fluorescein diacetate probe (DCF-H2-DA) (Sigma-Aldrich) for 45 min at 37°C. The non-fluorescent DCF-H2-DA probe transforms after hydrolysis by cellular esterases and oxidation by ROS into 2',7'-dichlorofluorescein, which emits green fluorescence that can be detected at 525 nm when excited at 488 nm emission wavelengths [24]. After the incubation time, the cells were washed again with PBS, incubated with trypsin-EDTA and re-suspended in a new supplemented culture medium at 4°C. Control samples corresponding to cells incubated without MoS_2 flakes were included in the assays. ROS production was analyzed by flow cytometry using the same equipment and software described in the previous section.

2.6. ALP activity

MC3T3-E1 preosteoblasts have the capacity to differentiate into osteoblasts and osteocytes and have been demonstrated to secrete collagen and form calcified bone tissue *in vitro* [25]. Ascorbic acid is extremely important for the differentiation of osteoblasts since it is a cofactor for the synthesis of collagen allowing the formation of the collagen matrix which is necessary for the induction of differentiation markers, such as alkaline phosphatase (ALP) [26]. ALP activity was measured to evaluate the effect of the incorporation of nucleotide-stabilized MoS_2 flakes on cell differentiation of

osteoblast cells. To this end, MC3T3-E1 preosteoblasts, as undifferentiated osteoblast-like cells were seeded with a cell density of 5×10^3 cells in 2 mL^{-1} in MEM Alpha medium supplemented with 10% fetal bovine serum, 1 mM L-glutamine, penicillin (800 $\mu g\ mL^{-1}$), streptomycin (800 $\mu g\ mL^{-1}$), ascorbic acid and glycerophosphate under CO_2 (5%) in humidified atmosphere at 37ºC for 24 h. Subsequently, the culture medium was replaced by a fresh one containing 50 $\mu g\ mL^{-1}$ of the nanomaterials and the cells incubated for 10 days, replacing their culture medium every two days. Control samples corresponding to cells cultured in the absence of MoS_2 were included in the assays. To get direct evidence of the cell morphology after nanomaterials incorporation as well as their intracellular localization, the cells were observed by inverted optical microscopy (Eclipse TS 100, Nikon; Digital Sight DS-2Mv).

ALP activity was measured using the Reddi and Huggins method based on the hydrolysis of *p*-nitrophenyl phosphate (pNPP) in *p*-nitrophenol, one unit of ALP being defined as the enzyme activity that liberates 1 μmol of pNPP per 0.5 h under stated conditions [27]. The cells were washed with PBS and submitted to 3 cycles of freezing and thawing so that they were lysed before the enzymatic reaction, after which 10 mM *p*NPP was added and the cells were incubated for 30 min. Subsequently, 2M NaOH was added to stop the enzymatic reaction and the absorbance of pNPP was read at 405 nm on a spectrophotometer (GENESYS 20, USA). ALP activity was normalized as a function of total protein. The total protein was determined by the Bradford method using bovine serum albumin as standard. Thus, the total protein was quantified spectrophotometrically by measuring the absorbance at 595 nm of the anionic form of the dye Coomassie blue G250, which binds to the protein [28].

2.7. Statistical analysis

The data were expressed as the mean ± standard deviation (SD) of four independent experiments performed in triplicate. Statistical analysis was performed using Statistical Package for Social Sciences (SPSS, version19). The statistical comparisons between groups were made by analysis of variance (ANOVA) followed by the Scheffé test. Significant statistical differences were considered for values of $p<0.05$.

3. RESULTS AND DISCUSSION

3.1. Characterization of the MoS_2 dispersions

The MoS_2 flakes were obtained through exfoliation and colloidal stabilization of bulk MoS_2 powder in aqueous medium with the assistance of different nucleotides (AMP, GMP, FMN) as exfoliating/dispersing agents. Bath sonication of MoS_2 powder in aqueous solutions of the aforementioned nucleotides followed by mild centrifugation and purification yielded opaque, dark green dispersions indicative of successful exfoliation, which displayed long–term colloidal stability. In contrast, sonication and subsequent centrifugation of MoS_2 powder in water alone did not yield any significant amount of material in the supernatant. The successful exfoliation in water of MoS_2 was confirmed by the presence of the excitonic peaks characteristic of MoS_2 in its semiconducting 2H phase (Fig. S1D of the Supplementary Material), namely, the A, B, C and D bands locatedat ~670, 610, 450 and 400 nm, respectively, [20, 29-30] in the UV–vis extinction spectra of such dispersions (Figure 1G). It must be noted that nucleotide-stabilized MoS_2 flakes have a notable absorptive capacity in the infrared (wavelength above 800 nm). This has important implications for its potential biomedical uses, particullarly, in the context of photothermal therapy of tumors, which is, together with the use of MoS_2 as nano-vehicle for the transport of therapeutic agents, the subject of most current *in vitro* and *in vivo* research on this nanomaterial [31-36].

Specifically, previous studies in the literature test MoS_2 functionalized with the PEG polymer for such purposes. Photothermal therapy is an emerging therapeutic modality that uses energy-absorbing agents localized within tumor tissues and sources of Near-Infrared (NIR) light irradiation to generate heat, leading to the selective destruction of the tumor cells. The use of this irradiation in the 700–1100 nm range is particularly attractive, because biological systems mostly lack chromophores that absorb in the NIR region. Hence, if the NIR absorbing nanomaterial can be internalized by tumor cells, tumors can be selectively destroyed by a NIR laser emitting in the "therapeutical window".

The additional peaks in the 200–300 nm wavelength range were ascribed to UV absorption of the nucleotides (see the spectra of aqueous solutions of the nucleotides in Fig. S1A-C of the Supplementary Material) both adsorbed on the flakes and as free molecules in aqueous solution. The latter could be eliminated to a large extent by iterative cycles of sedimentation of the exfoliated MoS_2 material followed by re–suspension of the sediment in pure water. However, a small amount of nucleotide persisted in the purified dispersions, as indicated by the still visible bands in the wavelength range below 300 nm, which was obviously necessary for the colloidal stability of the exfoliated flakes. Indeed, although additional sedimentation/re–suspension cycles afforded further elimination of the nucleotide, the colloidal stability of the purified dispersion was concomitantly reduced. Two cycles were found to be a reasonable compromise between purification and colloidal stability of the dispersions. The presence of the nucleotides adsorbed on the MoS_2 flakes was also confirmed in a previous work by atomic force microscopy. Indeed, the appearance of discrete features about 1 nm high on the surface of the MoS_2 flakes could be ascribed to the nucleotide molecules that remained adsorbed [19].

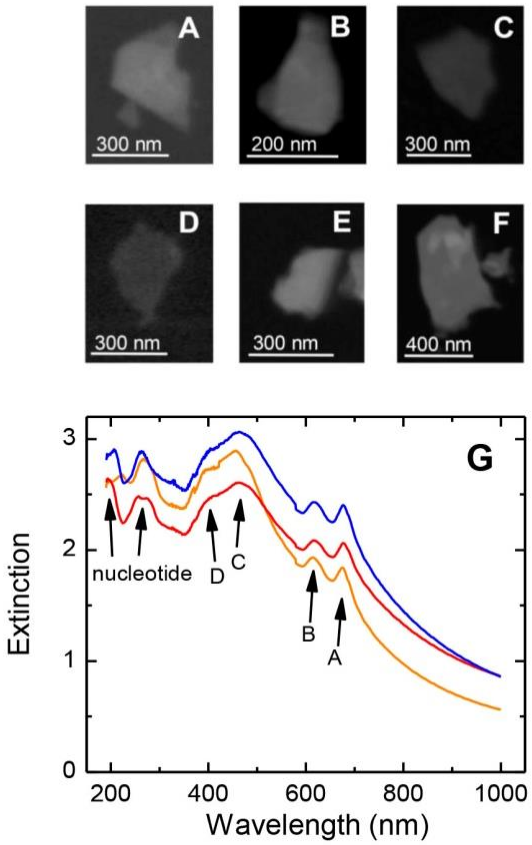

Figure 1. (A-F) Typical STEM images of MoS_2 flakes from aqueous dispersions stabilized by (**A, D**) AMP, (**B, E**) GMP and (**C, F**) FMN. **(G)** UV–vis extiction spectra of aqueous MoS_2 colloidal dispersions stabilized by AMP (blue trace), GMP (red trace) and FMN (orange trace). The excitonic peaks A, B, C and D characteristic of 2H–phase MoS_2 as well as some absorption bands of the nucleotides are indicated.

Recently, empirical formulae relating spectroscopic features of the extinction spectrum of MoS_2 dispersions to the lateral and vertical dimensions of the flakes have been made available. Specifically, the position of the A excitonic peak has been related to the average flake thickness, while the ratio of extinction at the B excitonic peak and the local minimum at 345 nm allows estimation of the mean lateral size of the flakes. Using such formulae, the average thickness and lateral size of the exfoliated flakes in the nucleotide–stabilized aqueous dispersions were estimated to be 9–10 monolayers and 250–300 nm, respectively. The lateral dimensions of the MoS_2 flakes directly observed by STEM (Figures 1A-F) were consistent with the latter values. Indeed, the

dispersions were observed to be mostly made up of lamellar objects of irregular polygonal shape with typical lateral sizes ranging in the 200–400 nm range.

The exfoliated MoS_2 flakes were further characterized by XPS. High resolution, core level Mo 3d and S 2p spectra of the flakes dispersed in AMP (blue trace), GMP (red trace) and FMN (orange trace) are given in Figures 2A and B, respectively. For the sake of comparison, the corresponding spectra of the starting, bulk MoS_2 powder are also shown (black traces). The starting bulk material displayed Mo 3d and S 2p features consistent with the thermodynamically stable 2H phase, specifically: Mo 3d doublet band with components located at ~229.3 and 232.5 eV, ascribed to the Mo^{4+} $3d_{5/2}$ and $3d_{3/2}$ levels of MoS_2, and S 2p doublet band with components at about 162.1 (S $2p_{1/2}$) and 163.3 (S $2p_{3/2}$) eV [37]. The nucleotide–exfoliated flakes displayed similar spectra shifted to higher binding energy values by 0.2–0.4 eVas a consequence of a charge effect, presumably due to the presence of adsorbed nucleotide molecules on the flakes and their relatively small lateral size. A hypothetical, partial structural transformation from 2H to 1Tpolymorph upon exfoliation can be ruled out on the basis of these XPS results, given that such a phase change would imply the emergence of components down shifted ~0.8eV in both the Mo 3d and S 2p spectra. Raman spectra provided additional endorsement to this conclusion. Indeed, the spectra of the flakes (Figure 2C) were similar to the spectrum of the starting bulk powder (black trace) and consistent with those expected for 2H MoS_2, showing only its characteristic A_{1g}, E_{2g} and E_{1g} bands at ~404cm^{-1},380 and 282cm^{-1}, respectively [38]. The slight (~5cm^{-1}) down–shift of all the peaks with respect to those of bulk MoS_2 is typically found for exfoliated MoS_2 flakes of small size and has been previously attributed to their relatively large fraction of edges. Taken together, the XPS and Raman spectroscopy results indicated that the

exfoliated flakes retained the structural and chemical integrity of their parent material throughout the preparation of the dispersions.

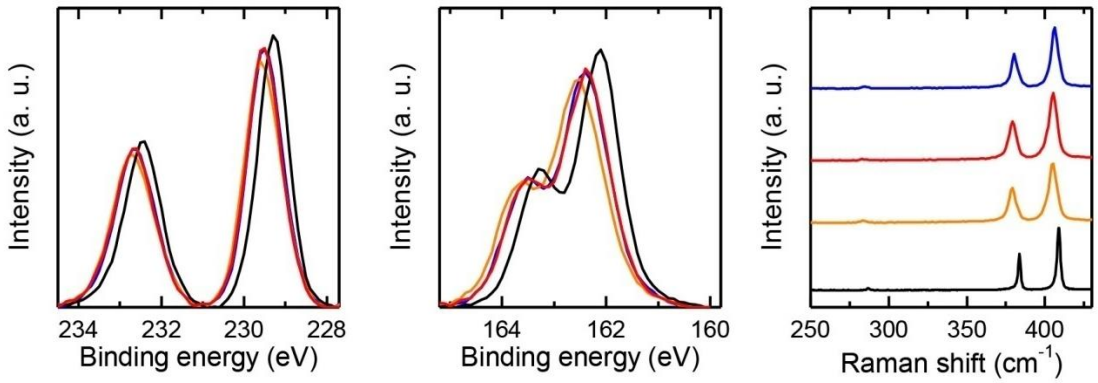

Figure 2. Normalized, background–subtracted, high resolution core level **(A)** Mo 3d and **(B)** S 2p XPS spectra of exfoliated MoS_2 with AMP (blue traces), GMP (red traces) and FMN (orange traces), as well as the starting, bulk MoS_2 powder (black traces). **(C)** Raman spectra of exfoliated MoS_2 flakes from dispersions stabilized with AMP (blue trace), GMP (red trace) and FMN (orange trace). The Raman spectrum of the starting, bulk MoS_2 powder has been added for comparison (black traces).

3.2. Cell viability and proliferation of MC3T3-E1 and Saos-2 cells exposed to nucleotide-stabilized MoS_2 dispersions

Cell viability is an important biological parameter related to the integrity of the cell membrane, which allows evaluating the biocompatibility of nanomaterials. Figure 3 displays the viability of MC3T3-E1 cells (Figure 3A) and Saos-2 cells (Figure 3B) when exposed to 10–75 μg mL^{-1} of nucleotide–stabilized MoS_2 flakes during 24 h. Both MC3T3-E1 cells (Figure 3A) and Saos-2 cells (Figure 3B) exposed to such nanomaterials showed high cell viability (≥90% and 95%, respectively), without significant differences with respect to control cells (100%).

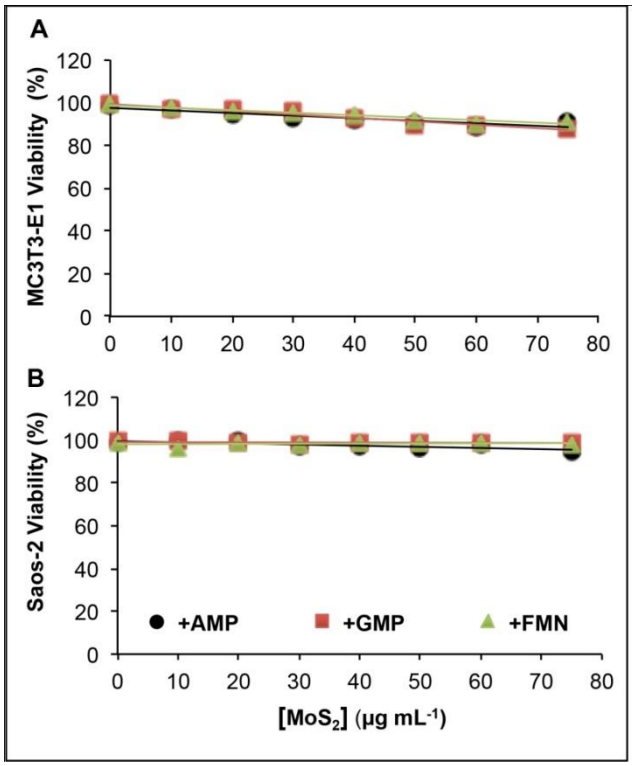

Figure. 3. Cell viability of the **(A)** MC3T3-E1 pre-osteoblasts and **(B)** Saos-2 human sarcoma osteoblasts exposed for 24 h at 10–75 µg mL^{-1} of MoS_2 flakes stabilized with AMP (black), GMP (red) and FMN (green), expressed as percentage of control cells (without flakes). The results are expressed as mean ± SD.

In addition to cell viability, another biological parameter widely used to test the biocompatibility of any nanomaterial is cell proliferation, which reflects the growth capacity of cells in the presence of nanomaterials. Figure 4 shows the proliferation of MC3T3-E1 cells (Figure 4A) and Saos-2 cells (Figure 4B) when exposed to 10–75 µg mL^{-1} of MoS_2 flakes stabilized with AMP, GMP and FMN mononucleotides during 24 h. On the one hand, MC3T3-E1 preosteoblasts growth capacity was found to be dependent on the concentration of MoS_2–AMP flakes. Indeed, this cell line possessed a similar proliferative capacity to that of control cells when exposed to 10 and 20 µg mL^{-1} of MoS_2–AMP flakes (Figure 4A, black line) but a significantly higher capacity when exposed to concentrations in the 30–75 µg mL^{-1} range (being 60%, 75%, 80%, 85% and 90% when compared to the proliferation of control cells for concentrations of 30, 40,

50, 60 and 75 μg mL^{-1}, respectively). On the other hand, the proliferative capacity of MC3T3-E1 cells exposed to MoS_2–GMP and MoS_2–FMN flakes for 24 h was similar to that shown by control cells for the whole range of studied concentrations. In the case of Saos-2 cells (Figure 4B), the proliferation capacity was similar in the absence (control samples) and in the presence of nucleotide–stabilized MoS_2 flakes irrespective of the nucleotide type (AMP, GMP or FMN) and for the whole range of concentrations (10–75 μg mL^{-1}).

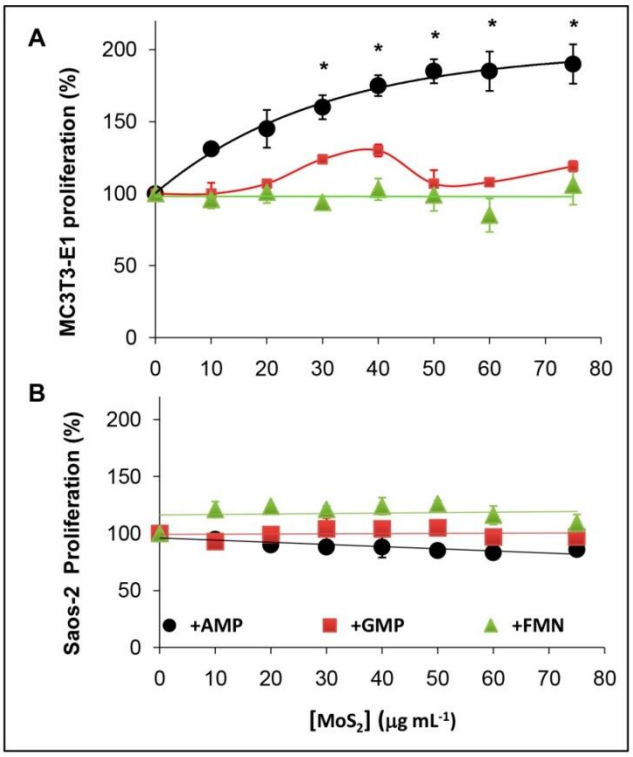

Figure. 4. Cell proliferation of the **(A)** MC3T3-E1 pre-osteoblasts and **(B)** Saos-2 human sarcoma osteoblasts exposed for 24 h at 10–75 μg mL^{-1} of MoS_2 flakes stabilized with AMP, GMP and FMN mononucleotide, expressed as percentage of control cells (cell proliferation in the absence of nanomaterials). The results are expressed as mean ± SD. *p <0.05.

This is, to the best of our knowledge, the first time that a comparative study of the cellular response of two cell lines (undifferentiated and tumor osteoblasts) exposed to a range of concentrations of MoS_2 flakes stabilized with different mononucleotides is carried out. MC3T3-E1 preosteoblasts and human Saos-2 osteoblasts have shown an

excellent biocompatibility when exposed to MoS_2 flakes stabilized with different small functional biomolecules such as AMP, GMP and FMN. It is important to remark that there is a difference clear between proliferations of MC3T3-E1 cells and Saos-2 cells after they were exposed to AMP-MoS_2 flakes. This fact could be due to the cellular characteristics that define one and another cell type. While the MC3T3-E1 preosteoblasts are immature cells with capacity to differentiate into osteoblasts and osteocytes, the Saos-2 cells are tumor osteoblasts with osteoblastic properties, making these cells a valuable model for studying events associated with the late osteoblastic differentitation stage. Moreover, MoS_2–AMP,–GMP and –FMN flakes in the tested concentrations allowed MC3T3-E1 and Saos cells proliferation, maintaining high cell viability. This is in agreement with previous studies in the literature, which report a good cell response of certain cell types when exposed to MoS_2 flakes functionalized with some stabilizers of amphiphilic nature, such as biocompatible polymers as PEG [39]. One of the potential advantages on the use of biomolecules as exfoliating/dispersing agents for TMDCs reported in this work is the smaller physical dimensions of these natural stabilizers compared to those of polymers, which, could, in principle, enhance the cellular uptake process for purposes such as cell labeling and drug/gene delivery directly into cells. Furthermore, not only the size, but also the nature of the stabilizers could enhance the cellular uptake processes. Indeed, nano-bio interface interactions are highly important in the biomedical sciences, because they determine the nanomaterials design with unique physicochemical properties such as hydrophilicity, hydrophobicity, size (side dimension), surface properties (functionalization), among other. These properties have an influence on the cellular uptake, transport, bioavailability, and final destination of the nanomaterials inside the biological systems [40]. To check if such a cellular uptake enhancement takes place, we quantitavely

evaluated the incorporation of nucleotide-stabilized MoS_2 flakes by MC3T3-E1 preosteoblasts and human Saos-2 cells.

3.3. Cellular internalization of nucleotide-stabilized MoS_2 flakes

Flow cytommetry is a method widely used to evaluate the potential of incorporation of nanomaterials by mammalian cells [41,42] through the evaluation of changes in the flow cytometric side-scatter intensity [22]. In many cases, after interacting with receptor targets in the cellular plasma membrane, nanomaterials are incorporated into cells via endocytosis. For the cellular incorporation assay and basing on the proliferative capacity reported above, we chose two concentrations (10 and 50 μg mL^{-1}) as representative of the whole concentration range (10–75 μg mL^{-1}). Specifically, 10 μg mL^{-1} corresponds to the minimal concentration of MoS_2 flakes tested in which both cell types had a similar proliferative capacity, whereas 50 μg mL^{-1} represents a MoS_2 flakes concentration in which Saos-2 cells and MC3T3-E1 preosteoblasts had a different proliferative response. As for the choice of representative times to permit their incorporation, we could not rely on previous kinetic studies on the cellular incorporation process of nucleotide-stabilized MoS_2 flakes, as, to the best of our knowledge, they are not available. However, the cellular incorporation of nanomaterials with similar sizes to that presented by our MoS_2 flakes has been reported to take place in a time range from 2 to 24 h [43], from which 4 and 24 h were chosen as representative times to guarantee their incorporation. Cellular endocytotic processes are intrinsically temperature-dependent. In fact, active internalization is suppressed below 4ºC [44]. Thus, to confirm the incorporation of the nucleotide-stabilized MoS_2 flakes and distinguish it from possible simple adhesion to the outer cell membrane, we performed some additional experiments where the endocytosis process was inhibited in one set of samples by cell incubation with the nanomaterials at 4ºC (data not shown).

Figure 5 represents the cellular incorporation of MoS_2-AMP (A), MoS_2-GMP (B) and MoS_2-FMN (C) flakes by MC3T3-E1 preosteoblasts. Figure 5A, 5B and 5C, show representative scatter plots of the cell size (FSC) of three cell populations, as a function of their internal complexity (SSC). In all the diagrams, black population represents the control cells (without nanomaterial), blue population represents MC3T3-E1 cells exposed for 24 h to 10 μg mL^{-1} of MoS_2–AMP (Figure 5A), MoS_2–GMP (Figure 5B) and MoS_2–FMN (Figure 5C), respectively, and red population represents the MC3T3-E1 cells exposed for 4 h at 50 μg mL^{-1} of MoS_2–AMP (Figure 5A), MoS_2–GMP (Figure 5B) and MoS_2–FMN (Figure 5C), flakes respectively. The insets of Figures 5A, 5B and 5C show the SSC expressed as mean ± SD for the conditions tested.

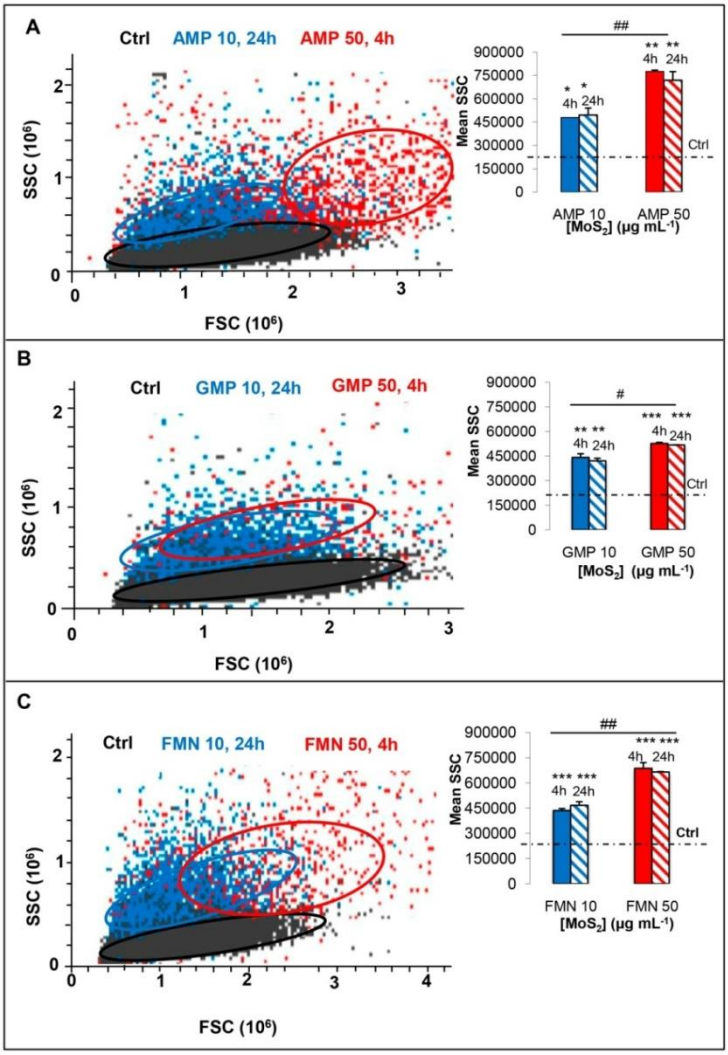

Figure 5. Cellular internalization of nucleotide-stabilized MoS_2 flakes by MC3T3-E1 cells. Representative scatter plot of FSC *versus* SSC of MC3T3-E1 pre-osteoblasts when exposed to **(A)** MoS_2-AMP:10 μg mL^{-1} for 24 h (blue) and 50 μg mL^{-1} for 4 h (red), **(B)** MoS_2-GMP:10 μg mL^{-1} for 24 h (blue) and 50 μg mL^{-1} for 4 h (red) and **(C)** MoS_2-FMN:10 μg mL^{-1} for 24 h (blue) and 50 μg mL^{-1} for 4 h (red). Control cells without nanomaterial maintained for 24 h (black). **(Inset)** SSC expressed in mean ± SD for the conditions tested. *p <0.05, **p <0.01 and ***p <0.005, statistical differences compared to control cells. #p <0.05 and ##p <0.01, statistical differences between different concentrations at the same culture time.

Regarding to MoS_2–AMP flakes incorporation (Figure 5A), the results indicate that the internal cellular complexity (SSC) of MC3T3-E1 preosteoblasts increases ≈88% and ≈95% compared to that of the control cells when exposed for 4 h and 24 h at 10 μg mL^{-1} of this nanomaterial, respectively. Furthermore, no significant differences were

observed when these cells were exposed to 10 μg mL^{-1} of MoS_2-AMP flakes during 4 and 24 h. Similarly, when MC3T3-E1 cells were exposed to 50 μg mL^{-1} of MoS_2-AMP for 4 h and 24 h an internal complexity increase (more than triple) compared to control cells was observed in both cases. Likewise, no significant differences were observed when these cells were exposed to 50 μg mL^{-1} of MoS_2-AMP flakes for 4 and 24 h. Thus, the maximal incorporation of 10 and 50 μg mL^{-1} of MoS_2-AMP flakes by MC3T3-E1 cells took place at exposure time of 4 h, for both concentrations, no further incorporation being observed as the culture time increased to 24 h. Finally, there also was a significant increase of ≈62% and ≈45%, in the internal complexity of MC3T3-E1 cells exposed for 4 h and 24 h, respectively, to 50 μg mL^{-1} of MoS_2-AMP flakes compared to those shown by cells exposed for the same times at a lower concentration (10 μg mL^{-1}).

Concerning to MoS_2-GMP flakes incorporation by MC3T3-E1 cells, the results shown in Figure 5B reveal a similar behavior to that shown in the MoS_2-AMP flakes incorporation. MoS_2-GMP flakes incorporation by the cells is observed at the two exposure times tested (4 and 24 h) and nanomaterial concentrations (10 and 50 μg mL^{-1}) assayed. Indeed, a significant increase of ≈73% and ≈66% in the SSC was observed when MC3T3-E1 cells were exposed to 10 μg mL^{-1} of this nanomaterial for 4 and 24 h, respectively, compared to the control cells. Likewise, when exposed to 50 μg mL^{-1} of MoS_2-GMP for both 4 h and 24 h, the cellular complexity of MC3T3-E1 cells significantly increases (more than double in both cases) compared to that of control cells. Similarly to that previously observed with the MoS_2-AMP nanomaterial we found that the maximal MoS_2-GMP incorporation by preosteosblasts was obtained after 4 h of exposure for both concentrations tested (10 and 50 μg mL^{-1}), there being no more incorporation as the culture time increased to 24 h. Finally, there also was a significant

increase of ≈19% and ≈23%, in the internal complexity of MC3T3-E1 cells exposed for 4 h and 24 h, respectively, to 50 μg mL^{-1} of MoS_2-GMP flakes compared to those shown by cells exposed for the same times at a lower concentration (10 μg mL^{-1}) of nanomaterial.

The MoS_2-FMN flakes incorporation is shown in Figure 5C, revealing that 10 and 50 μg mL^{-1} of these flakes were also incorporated by MC3T3-E1 preosteoblasts at the two exposure times tested (4 h and 24 h). A significant increase of ≈71% and ≈84% in the internal complexity was observed when cells were exposed to 10 μg mL^{-1} of this nanomaterial for 4 h and 24 h, respectively, compared to the control cells. Likewise, when MC3T3-E1 cells were exposed to 50 μg mL^{-1} of MoS_2-FMN for 4 h and 24 h, in both cases, significantly increased their cellular internal complexity (more than double) compared to control cells. In this case, similarly to those previously described, we observed a maximal MoS_2-FMN flakes incorporation after 4 h of exposure for both concentrations tested (10 and 50 μg mL^{-1}), there being no more incorporation as the culture time increased to 24 h. Finally, the internal complexity of MC3T3-E1 cells exposed to 50 μg mL^{-1} of MoS_2-FMN flakes for 4 h and 24 h significantly increase ≈57% and ≈42%, respectively, compared to those obtained by cells exposed for the same times at a lower concentration of nanomaterial (10 μg mL^{-1}).

From these results we can conclude that the incorporation of MoS_2 flakes stabilized with AMP, GMP and FMN mononucleotides by MC3T3-E1 preosteoblasts is higher as the nanomaterial concentration increases and it is independent of exposure time, since the maximal incorporation was obtained after 4 h for both concentrations tested (10 and 50 μg mL^{-1}), there being no more incorporation as the culture time increased to 24 h. Moreover, taking into account the high viability percentages obtained

(Figure 3A) we can conclude that the incorporation of these flakes does not alter the membrane plasma integrity of this cell type.

Figure 6 shows representative intracellular complexity (SSC) profiles *versus* number of Saos-2 cells of different cell populations exposed to 10 μg mL^{-1} of (A) MoS_2-AMP, (C) MoS_2-GMP and (E) MoS_2-FMN for 4 h (blue) and 24 h (red) and exposed to 50 μg mL^{-1} of (B) MoS_2-AMP, (D) MoS_2-GMP and (F) MoS_2-FMN for 4 h (blue) and 24 h (red). Control cells without nanomaterial appear always in black. Inset of each profile shows the SSC expressed as mean ± SD for the conditions tested. Results shows a clear shift to the right of the intracellular complexity profiles in all studied conditions compared to control cells, indicating an increase of this parameter. Specifically, cells exposed to 10 μg mL^{-1} of MoS_2-AMP flakes for 4 and 24 h (Figure 6A) increased significantly ≈18% and ≈98%, respectively, their internal complexity compared to that shown by control cells. Moreover, it is important to note that the SSC parameter of Saos-2 cells increased significantly ≈66% as increased the exposure time (24 h) to this nanomaterial concentration (10 μg mL^{-1}). Thus, these results demonstrate that the incorporation of these flakes increases with the exposure time. Similarly, cells exposed to 50 μg mL^{-1} of MoS_2-AMP flakes for 4 and 24 h (Figure 6B) increased significantly ≈70% and more than double, respectively, their internal complexity compared to that shown by cells cultured without nanomaterial. Furthermore, Saos-2 cells exposed to the higher MoS_2-AMP flakes concentration (50 μg mL^{-1}) for 24 h also significantly increased ≈70% their internal complexity compared to that shown by osteoblasts cultured for a lower time (4 h).

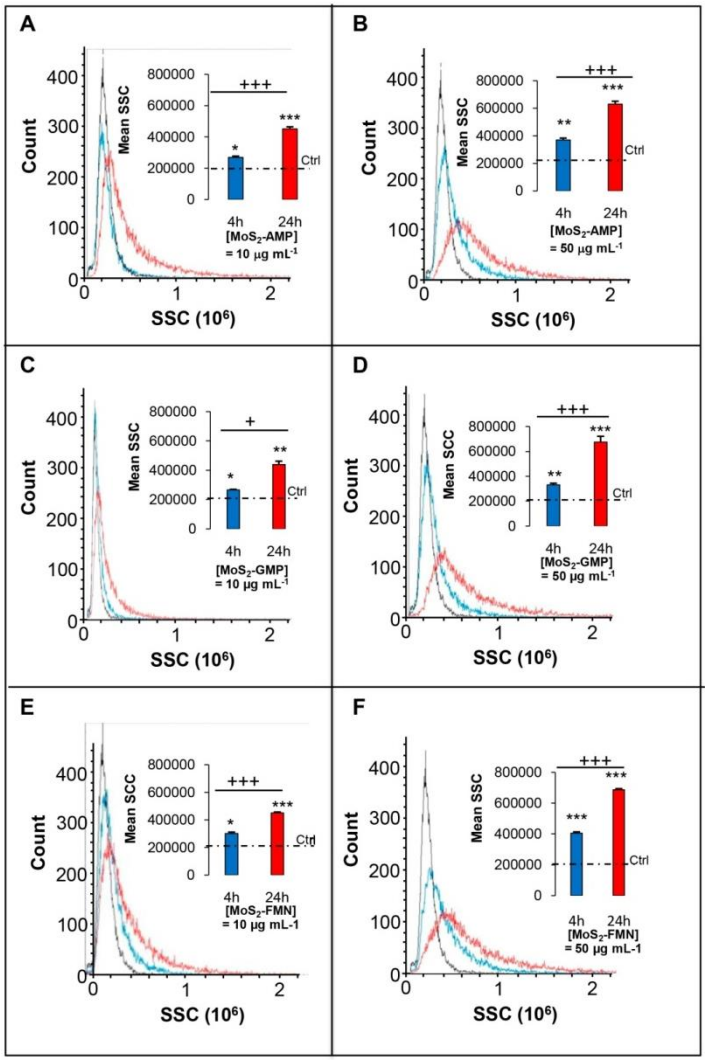

Figure 6. Cellular internalization of nucleotide-stabilized MoS_2 flakes by Saos-2 cells. Representative cellular complexity (SSC) profile *versus* number of Saos-2 cells exposed to 10 µg mL^{-1} of (**A**) MoS_2-AMP, (**C**) MoS_2-GMP and (**E**) MoS_2-FMN for 4 h (blue) and 24 h (red). Representative cellular complexity (SSC) profile *versus* number of Saos-2 cells exposed to 50 µg mL^{-1} of (**B**) MoS_2-AMP, (**D**) MoS_2-GMP and (**F**) MoS_2-FMN for 4 h (blue) and 24 h (red). (**Inset**) SSC expressed as mean ± SD for the conditions tested. Control cells (black) cultured with nanomaterial. *p <0.05, **p <0.01 and ***p <0.005, statistical differences compared to control cells. $^{+}$p <0.05, $^{++}$p <0.01 and $^{+++}$p <0.005, statistical differences comparing different culture times.

Internal complexity of human Saos-2 osteoblasts exposed to 10 µg mL^{-1} of MoS_2-GMP flakes (Figure 6C) for 4 h (blue column) and 24 h (red column) and exposed to 10 µg mL^{-1} of MoS_2-FMN (Figure 6E) for the same times, significantly increased ≈16%, ≈92%, ≈31% and ≈97%, respectively, compared to that shown by

control osteoblasts. Additionally, when osteoblasts were exposed to 10 μg mL^{-1} of MoS_2-GMP (Figure 6C) and 10 μg mL^{-1} of MoS_2-FMN flakes (Figure 6E) for a higher exposure time (24 h, red column), their SSC also significantly increased ≈65% and ≈49%, respectively, compared to that shown by Saos-2 cells cultured for a lower time (4 h).

As regards the internal complexity of human Saos-2 osteoblasts, those of cells exposed to 50 μg mL^{-1} of MoS_2-GMP (Figure 6D) for 4 h (blue column) and 24 h (red column) and exposed to 50 μg mL^{-1} of MoS_2-FMN (Figure 6F) for the same times, significantly increased ≈45%, more than double, ≈77% and more than triple, respectively, compared to that shown by control osteoblasts. Additionally, when osteoblasts were exposed to 50 μg mL^{-1} of MoS_2-GMP (Figure 6D) and 50 μg mL^{-1} of MoS_2-FMN (Figure 6F) for a higher exposure time (24 h, red column), their SSC also significantly increased more than double and ≈69%, respectively, compared to that shown by Saos-2 cells cultured for a lower time (4 h). From these results, and unlike what happened with MC3T3-E1 preosteoblasts (undifferentiated cells), we can conclude that the MoS_2 flakes incorporation stabilized with mononucleotides, AMP, GMP and FMN by tumor cells (human Saos-2 osteoblasts) is higher as the nanomaterial concentration and the exposure time increases. Thus, the maximal nanomaterial incorporation was obtained after 24 h of exposure to the higher concentration tested, *i.e.* 50 μg mL^{-1}, in all studied conditions. Once more, the incorporation of these flakes does not alter the membrane plasma integrity of Saos-2 osteoblasts since high viability percentages were obtained by this cell type (Figure 3B) when exposed to these nanomaterials.

As mentioned above, MoS_2 flakes stabilized with different agents are being proposed for a great variety of biomedical applications such as photothermal therapy,

nano-vehicles of genes for transfection process and, as nano-vehicles of drugs for which, flakes have to be incorporated by the cells without causing structural or functional alterations. Our results show that MoS_2 flakes stabilized with AMP, GMP and FMN mononucleotides and with a lateral size of 200–400 nm are incorporated by tumor cells and undifferentiated cells following different patterns (time exposure and concentration), what provides valuable information for the final biomedical application of the nanomaterial. Taking into account that our nucleotide-stabilized MoS_2 flakes have a notable absorptive capacity in the infrared and that these flakes are perfectly incorporated by tumor cells, they can be proposed as candidates for photothermal therapy, acting as photothermic agents at the sub-cellular level. As mentioned above, the 2D MoS_2 nanomaterial have been also purposed as a drug delivery nano-vehicle. In this sense, given the results of viability, proliferation and cellular incorporation obtained with both tumor cells (Saos-2) and with undifferentiated healthy cells (MC3T3-E1 preosteoblasts), the nucleotide-stabilized MoS_2 flakes presented here, could also be proposed as new nano-vehicles functionalized with biological molecules, what could be an added value. Anyhow, more specific studies would be necessary to check the actual performance of our nanomaterials in each intended application.

3.4. Reactive oxygen species production by MC3T3-E1 and Saos-2 cells exposed to nucleotide-stabilized MoS_2 flakes

Several studies have proposed oxidative stress as a key mechanism involved in the toxicity of several nanomaterials resulting from the imbalance between the excessive production of reactive oxygen species (ROS) and the limited capacity of the antioxidant defenses of the cells, leading to adverse biological effects such as membrane lipid peroxidation, protein denaturation and DNA changes [45]. ROS include a number of

molecules that damage DNA and RNA and oxidize proteins and lipids (lipid peroxidation). These reactive molecules contain oxygen and include H_2O_2 (hydrogen peroxide), NO (nitric oxide), O_2^- (superoxide anion), peroxynitrite ($ONOO^-$), hydrochlorous acid (HOCl) and hydroxyl radical (OH^-) [46]. Figure 7 shows ROS production by MC3T3-E1 preosteoblasts (Figure 7A) and Saos-2 osteoblasts (Figure 7B) exposed to 10 and 50 μg mL^{-1} of MoS_2-AMP, MoS_2-GMP and MoS_2-FMN flakes for 24 h. Concerning the ROS production by MC3T3-E1 cells, the results show that only preosteoblasts exposed to 10 and 50 μg mL^{-1} of MoS_2-AMP flakes increased significantly their ROS production ≈32 and ≈31%, respectively, compared to that shown by preosteoblasts cultured without nanomaterial. This fact could be related to the significant increase in MC3T3-E1 cell proliferation (Figure 4A) when they were exposed to MoS_2-AMP flakes for 24 h. So, the ROS production increase would be due to the high cell density, without involving cytotoxicity of the flakes. Moreover, it is important to highlight the high percentages of cell viability were obtained (Figure 3A). On the other hand, no significant differences were observed in the ROS production by MC3T3-E1 cells when exposed to MoS_2-GMP and MoS_2-FMN flakes, except in the case of those cells exposed to the higher concentration of MoS_2-GMP nanomaterial (50 μg mL^{-1}) where a significant decrease (≈34%) in their ROS production is observed.

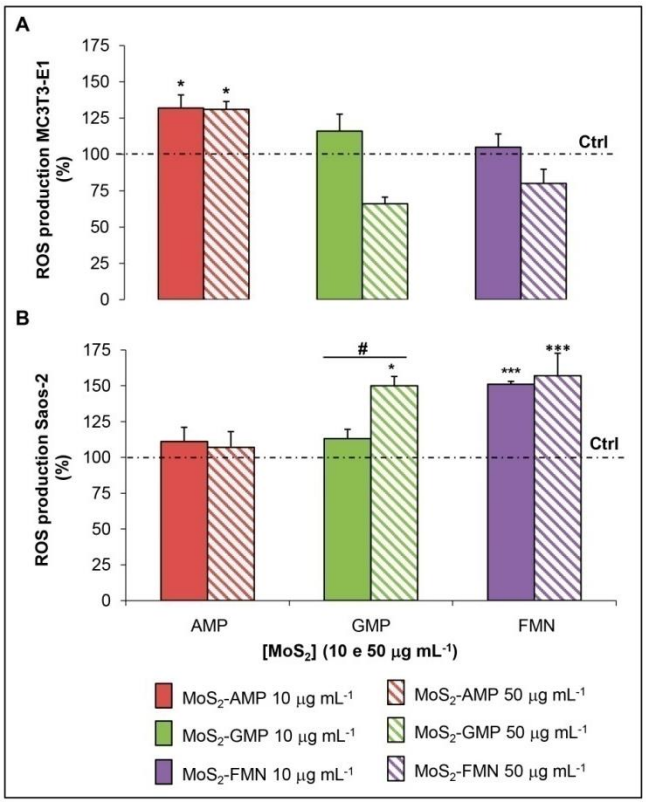

Figure 7. Percentage of ROS production by **(A)** MC3T3-E1 preosteoblasts and **(B)** Saos-2 osteoblasts exposed to 10 μg mL^{-1} of MoS_2-AMP (red), MoS_2-GMP (green), MoS_2-FMN flakes (purple) and exposed to 50 μg mL^{-1} of MoS_2-AMP (red stripes), MoS_2-GMP (green stripes) and MoS_2-FMN flakes (purple stripes) for 24 h. Results (mean ± SD) are expressed as % of the control (black dashedline). *p <0.05 and ***p <0.005, statistical differences compared to control cells. #p <0.05, statistical differences comparing different concentrations of the nanomaterial.

Concerning to the ROS production by Saos-2 osteoblasts, when this cell type was exposed to the higher MoS_2-GMP concentration (50 μg mL^{-1}), and to 10 μg mL^{-1} and 50 μg mL^{-1} of MoS_2-FMN, there is a significant increase of ≈50%, ≈52% and ≈56%, respectively, compared to that shown by control cells. These results are in agreement with other studies which demonstrated that MoS_2 flakes functionalized with biocompatible polymers as PEG or PEG-PEI induced minimal oxidative stress [47]. On the other hand, the ROS production increase by MC3T3-E1 cells takes place when exposed to MoS_2-AMP flakes. However, in the case of Saos-2 osteoblasts, there is a

ROS production increase when exposed to MoS_2-GMP and MoS_2-FMN flakes. Therefore, our results also demonstrated that the ROS production by tumor cells (Saos-2 osteoblasts) and by undifferentitated preosteoblasts (MC3T3-E1) could be related to the biomolecule used as dispersing/stabilizing agent (AMP, GMP and FMN mononucleotides) in the colloidal dispersion of MoS_2 flakes.

3.5. Alkaline phosphatase activity of MC3T3-E1 cells after internalization of nucleotide-stabilized MoS_2 flakes

The osteoblastic cell line MC3T3-E1 is characterized by having high alkaline phosphatase (ALP) activity in the resting state. ALP is a glycoprotein present on the surface of the cell that is detected in the early stages of the differentiation process and is involved in the mineralization process. These cells have also the capacity to differentiate into osteoblasts and osteocytes [25]. Figure 8 shows a representative image of the MC3T3-E1 preosteoblasts morphology after MoS_2 flakes incorporation (Figure 8A, 8B, 8C and 8D) and their ALP activity when exposed to 50 μg mL^{-1} of MoS_2-AMP, MoS_2-GMP and MoS_2-FMN flakes for 10 days (Figure 8E). This concentration was chosen in order to verify if a high concentration of this nanomaterial inside the cells could affect the first stage of the cell differentiation process (namely known as early stage). MC3T3-E1 cells show a fibroblast-like morphology, typical of this cell type and are able to grow in adherent monolayer. Moreover, this cell type appeared ‘‘healthy’’, *i.e.*, no modification of their morphology was found when compared to untreated control cells. In addition, cell distribution of the nanomaterials is critically dependent on the cell type and their lateral dimension, among other parameters. In this study, we observe that MoS_2 flakes stabilized with different mononucleotides (AMP, GMP and FMN) were internalized by the cells, being preferentially localized in the perinuclear

area (as indicated by arrows), clearly outside of the nucleus and no apparent signs of nuclear shrinkage (pyknosis) was observed.

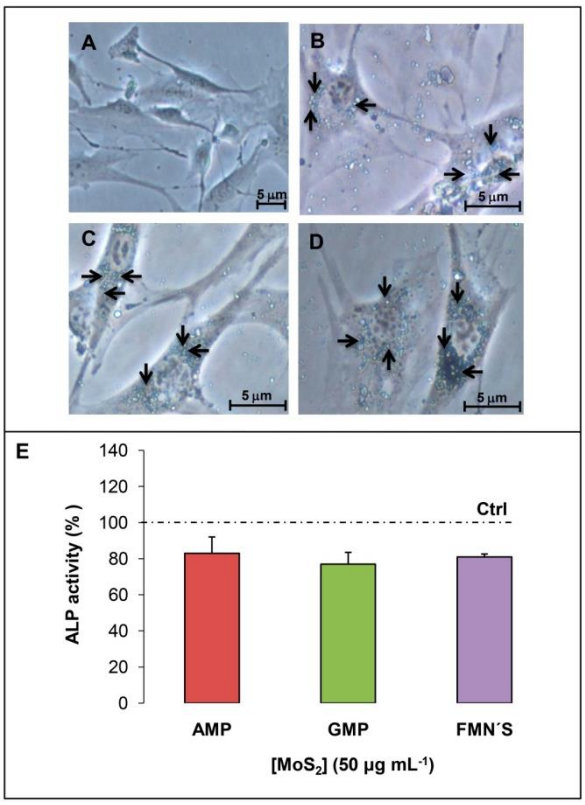

Figure 8. Morphological evaluation of MC3T3-E1 cells after exposure at 50 μgmL^{-1} of **(B)** MoS_2-AMP, **(C)** MoS_2-GMP and **(D)** MoS_2-FMN flakes evaluated by optical microscopy. Control cells (absence of nanomaterial) were always carried out **(A)**. The arrows indicate the location of nanomaterials inside the cells. **(E)** Evaluation of the differentiation capacity of the MC3T3-E1 cell line. ALP activity em percentage in function of the total protein of MC3T3-E1 preosteoblasts exposed for 10 days to 50 μgmL^{-1} of MoS_2-AMP (red), MoS_2-GMP (green) and MoS_2-FMN (purple). The results (mean ± SD) are expressed as % of the control (black dashed line).

Finally, no significant differences are found in the ALP activity of MC3T3-E1 preosteoblasts exposed to MoS_2-AMP, MoS_2-GMP and MoS_2-FMN flakes for 10 days compared to that shown by preosteoblast cultured without nanomaterial (Figure 8E). To the best of our knowledge, this is the first report on the differentiation ability (early stage) of MC3T3-E1 preosteoblasts exposed to MoS_2 flakes stabilized with

mononucleotides. Our results provide relevant information for future biomedical applications of these materials although more specific studies would be necessary for each potential application.

4. CONCLUSIONS

An attractive means to favor the interaction of MoS_2 flakes with biological media is the use of proper biomolecules as exfoliating/dispersing agents. Here, MoS_2 flakes were stabilized with different small functional biomolecules such as AMP, GMP and FMN mononucleotides through the strong nucleotide−MoS_2 interaction of Lewis acid-base type, rather than just on the weak dispersive and hydrophobic forces commonly associated with the use of many surfactants. Moreover, these MoS_2 flakes showed an excellent biocompatibility with MC3T3-E1 preosteoblasts and human Saos-2 osteoblasts, allowing their cell proliferation and maintaining high cell viability. For both types of cells, the incorporation of these 2D nanomaterials was higher as the nanomaterial concentration increased and did not alter their membrane plasma integrity in the concentration range under study. However, the flakes incorporation was higher as the exposure time increased in the case of human Saos-2 osteoblasts (tumor cells) while it was independent of exposure time for MC3T3-E1 preosteoblasts. Results also revealed that the ROS production by both cell types could be related to the biomolecule used as dispersing/stabilizing agent (AMP, GMP and FMN mononucleotides) in the colloidal dispersion of MoS_2 flakes. Finally, the early stage of the preosteoblast cell differentiation process (ALP enzimatic activity) was not affected when MC3T3-E1 preosteoblasts were exposed to these MoS_2 flakes for 10 days. Basing on these results, nucleotide-stabilized MoS_2 flakes can be proposed as candidates for photothermal therapy, and as nano-vehicles for the transport of therapeutic agents at the sub-cellular level.

Acknowledgments

M. Cicuéndez. acknowledges the FCT financial support [Post-Doctoral Grant SFRH/BPD/101468/2014] and Operational Program Human Capital (POCH), European Union. V.S. Silva acknowledges financial support from the FCT [SFRH/BPD/110269/2015 Post-Doctoral grant]. H. Oliveira. acknowledges financial support FCT SFRH/BPD/111736/2015. M. A.-V., S. V.-R. and J. I. P gratefully acknowledge financial support from the Spanish Ministerio de Economía y Competitividad (MINECO) and the European Regional Development Fund (ERDF) through project MAT2015-69844-R. Partial funding by Plan de Ciencia, Tecnología e Innovación (PCTI) 2013-2017 del Principado de Asturias and the ERDF (project GRUPIN14-056) is also acknowledged. M.A-V. is grateful to MINECO for his pre-doctoral contract.

References

[1] Y. Chen, C. Tan, H. Zhang, L. Wang. Two-dimensional graphene analogues for biomedical applications. Chem. Soc. Rev. (2015), 44, 2681–2701.

[2] Y. Yong, L. Zhou, Z. Gu, L. Yan, G. Tian, X. Zheng, X. Liu, X. Zhang, J. Shi, W. Cong. WS_2 nanosheet as a new photosensitizer carrier for combined photodynamic and photothermal therapy of cancer cells. Nanoscale (2014), 6, 10394–10403.

[3] M. Xiao, A.R. Chandrasekaran, W. Ji, F.Li, T. Man, Ch. Zhu, X. Shen, H. Pei, Q. Li, L. Li. Affinity-Modulated Molecular Beacons on MoS2 Nanosheets for MicroRNA Detection. ACS Appl. Mater. Interfaces (2018), 10, 35794-35800.

[4] M. Xiao, T. Man, C. Zhu, H. Pei, J. Shi, L. Li, X. Qu, X. Shen, J. Li. MoS2 Nanoprobe for MicroRNA Quantification Based on Duplex-Specific Nuclease Signal Amplification. ACS Appl. Mater. Interfaces (2018), 10, 7852-7858.

[5] R. Zhong, Q. Tang, S. Wang, H. Zhang, F. Zhang, M. Xiao,T. Man, X. Qu, L. Li, W. Zhang, H. Pei. Self-Assembly of Enzyme-Like Nanofibrous G-Molecular Hydrogel for Printed Flexible Electrochemical Sensors. Adv. Mater. (2018), 30, 1706887.

[6] L. Qi, M. Xiao, X. Wang, C. Wang, L. Wang, S. Song, X. Qu, L. Li, J. Shi, H. Pei. DNA-Encoded Raman-Active Anisotropic Nanoparticles for microRNA Detection. Anal. Chem. (2017), 89, 9850−9856.

[7] L. Qi, M. Xiao, F. Wang, L. Wang, W. Ji, T. Man, A. Aldalbahi, M. Naziruddin Khan, G. Periyasami, M. Rahaman, A. Alrohaili, X. Qu, H. Pei, C. Wang, L. Li. Poly-ytosine-mediated nanotags for SERS detection of Hg2+. Nanoscale (2017), 9, 14184–14191.

[8] L. Chen, J. Chao, X. Qu, H. Zhang, D. Zhu, S. Su, A. Aldalbahi, L. Wang, H. Pei. Probing Cellular Molecules with PolyA-Based Engineered Aptamer Nanobeacon. ACS Appl. Mater. Interfaces (2017), 9, 8014−8020.

[9] D. Zhu, P. Song, J. Shen, S. Su, J. Chao, A. Aldalbahi, Z. Zhou, S. Song, C. Fan, X. Zuo, Y. Tian, L. Wang, H. Pei. PolyA-Mediated DNA Assembly on Gold Nanoparticles forThermodynamically Favorable and Rapid Hybridization Analysis. Anal. Chem. (2016), 88, 4949−4954.

[10] G. Yao, H. Pei, J. Li, Y. Zhao, D. Zhu, Y. Zhang, Y. Lin, Q. Huang, C. Fan. Clicking DNA to gold nanoparticles:poly-adenine-mediated formation of monovalent DNA-gold nanoparticle conjugates with nearly quantitative yield. NPG Asia Materials (2015) 7, e159.

[11] T. Liu, C. Wang, X. Gu, H. Gong, L. Cheng, X. Shi, L. Feng, B. Sun, Z. Liu. Drug delivery with PEGylated MoS2 Nano-sheets for combined photothermal and chemotherapy of cancer. Adv. Mater. (2014), 26, 3433–3440.

[12] Z. Li, S.L. Wong. Functionalization of 2D Transition Metal Dichalcogenides for Biomedical Applications. Mater. Sci. Eng. C (2017), 70, 1095-1106.

[13] R. Jack Brent, N. Savjani, P. O'Brien. Synthetic approaches to two-dimensional transition metal dichalcogenide nanosheets. Prog. in Mater. Sci (2017), 89, 411–478.

[14] L. Guardia, J. I. Paredes, R. Rozada, S. Villar-Rodil, A. Martínez-Alonso, J. M. D. Tascón. Production of Aqueous Dispersions of Inorganic Graphene Analogues by Exfoliation and Stabilization with Non-Ionic Surfactants. RSC Adv. (2014), 4, 14115−14127.

[15] A. Gupta, V. Arunachalam, S. Vasudevan. Water Dispersible, Positively and Negatively Charged MoS_2 Nanosheets: Surface Chemistry and the Role of Surfactant Binding. J. Phys. Chem. Lett. (2015), 6, 739−744.

[16] N. D. Mansukhani, L. M. Guiney, P. J. Kim, Y. Zhao, D. Alducin, A. Ponce, E. Larios, M. J. Yacaman, M. C Hersam. High-Concentration Aqueous Dispersions of Nanoscale 2D Materials Using Nonionic, Biocompatible Block Copolymers. Small (2016), 12, 294−300.

[17] G. Guan, S. Zhang, S. Liu, Y. Cai, M. Low, C. P. Teng, I. Y. Phang, Y. Cheng, K. L. Duei, B. M Srinivasan, Y. Zheng, Y.-W. Zhang, M.-Y Han. Protein Induces Layer-by-Layer Exfoliation of Transition Metal Dichalcogenides. J. Am. Chem. Soc. (2015), 137, 6152−6155.

[18] G. S. Bang, S. Cho, N. Son, G. W. Shim, B.-K. Cho, S.-Y Choi. DNA-Assisted Exfoliation of Tungsten Dichalcogenides and Their Antibacterial Effect. ACS Appl. Mater. Interfaces (2016), 8, 1943−1950.

[19] M. Ayán-Varela, O. Pérez-Vidal, J. I. Paredes, J. M. Munuera, S. Villar-Rodil, M. Díaz-González, C. S. Fernández-Sánchez, V. S. Silva, M. Cicuéndez, M. Vila, A. Martínez-Alonso, J. M. D. Tascón. Aqueous Exfoliation of Transition Metal Dichalcogenides Assisted by DNA/RNA Nucleotides: Catalytically Active and Biocompatible Nanosheets Stabilized by Acid−Base Interactions. ACS Appl. Mater. Interfaces (2017), 9, 2835−2845.

[20] C. Backes, R.J. Smith, N. McEvoy, N.C. Berger, D. McCloskey, H.C. Nerl, A. O`Neill, P.J. King, T. Higgins, D. Hanlon, N. Scheuschner, J. Maultzsch, L. Houben,

G.S. Duesberg, J.F. Donegan, V. Nicolosi, J.N. Coleman. Edge and confinement effects allow in situ measurement of size and thickness of liquid-exfoliated nanosheets. Nat. Commun. (2014), 5, 4576.

[21] C. Greulich, J. Diendorf , T. Simon, G. Eggeler, M. Epple. Uptake and intracellular distribution of silver nanoparticles in human mesenchymal stem cells. Acta Biomater (2011), 7, 347-354.

[22] H. Suzuki, T. Toyooka, Y. Ibuki. Simple and Easy Method to Evaluate Uptake Potential of Nanoparticles in Mammalian Cells Using a Flow Cytometric Light Scatter Analysis Environ. Sci. Technol. (2007), 41, 3018-3024.

[23] J. N. Udall, R. A. Moscicki, F. I. Preffer, P. D. Ariniello, E. A. Carter, A. K. Bhan, K. J. Bloch. Flow Cytometry: A New Approach To The Isolation And Characterization Of Kupffer Cells. In: J. Mestecky et al. (eds.). Recent Advances in Mucosal Immunology. Plenum Press, New York 1987. pp 821-827.

[24] B. Halliwell, M. Whiteman. Measuring reactive species and oxidative damage in vivo and in cell culture: how should you do it and what do the results mean? British Journal of Pharmacology (2004) 142, 231–255.

[25] L. D. Quarles, D. A. Yohay, L. W. Lever, R. Caton, R. J. Wenstrup. Distinct Proliferative and Differentiated Stages of Murine MC3T3-E1 Cells in Culture: An In Vitro Model of Osteoblast Development. J. Bone Miner. Res. (1992), 7, 683−692.

[26] D. Wang, K. Christensen, K. Chawla, G. Xiao, P.H. Krebsbach, R. T. Franceschi. Isolation and Characterization of MC3T3-E1 Subclones with Distinct In Vitro and In Vivo Differentiation/Mineralization Potential. Journal of Bone and Mineral Research (1999), 14, 893-903.

[27] A. H. Reddi, C. Huggins. Biochemical Sequences in the Transformation of Normal Fibroblasts in Adolescent Rats. Proc. Nat. Acad. Sci. USA, (1972), 69, 1601-1605.

[28] N. J. Kruger, Ch. 3. The Bradford Method for Protein Quantitation In: Methods Molecular Biology, Vol 32. Basic Protein and Peptide Protocols. Edited by John M. Walker, Humana Press Inc., Totowa, New Jersey.

[29] D. Vella, V. Vega-Mayoral, C. Gadermaier, N. Vujicic, T. Borzda, P. Topolovsek, M. Prijatelj, I. Tempra, E. A. A. Pogna, G. Cerullo Femtosecond Spectroscopy on MoS_2 Flakes from Liquid Exfoliation: Surfactant Independent Exciton Dynamics. J. Nanophotonics (2016), 10, 012508.

[30] B.L. Li, H.L. Zou, L. Lu, Y. Yang, J.L. Lei, H. Q. Luo, N.B. Li. Dependent Optical Absorption of Layered MoS_2 and DNA Oligonucleotides Induced Dispersion Behavior

for Label-Free Detection of Single-Nucleotide Polymorphism. Adv. Funct. Mater. (2015), 25, 3541–3450.

[31] Z. Kou, X. Wang, R. Yuan, H. Chen, Q. Zhi, L. Gao, B. Wang, Z. Guo, X. Xue, W. Cao. A promising gene delivery system developed from PEGylated MoS_2 nanosheets for gene therapy. Nanoscale Research Letters (2014), 9, 587.

[32] W. Yin, L. Yan, J. Yu, G. Tian, L. Zhou, X. Zheng, X. Zhang, Y. Yong, J. Li, Z. Gu, Y. Zhao. High-Throughput synthesis of single-layer MoS2 nanosheets as a near-infrared photothermal-triggered drug delivery for effective cancer therapy. ACS Nano (2014), 8, 6922-6933.

[33] T. Liu, S. Shi, C. Liang, S. Shen, L. Cheng, C. Wang, X. Song, S. Goel, T.E. Barnhart, W. Cai. Iron oxide decorated MoS2 nanosheets with double PEGylation for chelater-free radiolabeling and multimodal imaging guided photothermal therapy. ACS Nano (2015) 9, 950-960.

[34] S. Wang, L. Li, Y. Chen, H. Chen, M. Ma, J. Feng, Q. Zhao, J. Shi. Biocompatible PEGylated MoS2 nanosheets: Controllable bottom-up synthesis and highly efficient photothermal regression of tumor. Biomaterials (2015) 39, 206-217.

[35] S. Wang, X. Li, Y. Chen, X. Cai, H. Yao, W. Gao, Y. Zheng, X. An, J. Shi, H. Chen. A facile one-pot synthesis of a two-dimensional MoS_2/Bi_2S_3 composite theranostic nanosystem for multi-modality tumor imaging and therapy. Adv. Mater. (2015), 27, 2775-2782.

[36] B. Huang, D. Wang, G. Wang, F. Zhang, L. Zhou. Enhancing the colloidal stability and surface functionality of molybdenum disulfide (MoS_2) nanosheets with hyperbranched polyglycerol for photothermal therapy. J. Colloid Interface Sci. (2017), 508, 214-221.

[37] G. Eda, H. Yamaguchi, D. Voiry, T. Fujita, M. Chen, M. Chhowalla, Photoluminiscence from Chemically Exfoliated MoS_2. Nano Lett. (2011), 11, 5111–5116.

[38] S. Jiménez Sandoval, D. Yang, R. F. Frindt, J. C. Irwin. Raman study and lattice dynamics of single molecular layers of MoS_2. Phys. Rev. B (1991), 44, 3955–3962.

[39] X. Wang, N.D. Mansukhani, L.M. Guiney, Z. Ji, Ch. Hyun Chang, M. Wang, Yu-Pei Liao, Tze-BinSong, B. Sun, R. Li, T. Xia, M.C. Hersam, A.E. Nel. Differences in the Toxicological Potential of 2D versus Aggregated Molybdenum Disulfide in the Lung. Small (2015), 11, 5079–5087.

[40] X.Q. Zhang, X. Xu, N. Bertrand, E. Pridgen, A. Swami, O.C. Farokhzad. Interactions of nanomaterials and biological systems: Implications to personalized nanomedicine. Adv. Drug Deliv. Rev. (2012), 64, 1363-1384.

[41] M. Kuchi, L. Diener, N. Bohmer, C. Hirsch, H.F. Krug, V. Palermo, P. Wick. Uptake of label-free graphene oxide by Caco-2 cells is dependent on the cell differentiation status. J. Nanobiotechnology (2017), 15, 46.

[42] F.F. Contreras-Torres, A. Rodríguez-Galván, C.E. Guerrero-Beltrán, E. Martínez-Lorán, E. Vázquez-Garza, N. Ornelas-Soto, G. García-Rivas. Differential cytotoxicity and internalization of graphene family nanomaterials in myocardial cells. Mater. Sci. Eng. C Mater. Biol. Appl. (2017), 73, 633-642.

[43] M. Vila, M.T. Portolés, P.A.A.P. Marques, M.J. Feito, M.C. Matesanz, C. Ramírez-Santillán, G. Gonçalves, S.M.A. Cruz, A. Nieto, M. Vallet-Regí. Cell uptake survey of pegylated nanographene oxide. Nanotechnology (2012), 23, 465103.

[44] M. Mahmoudi, *et al*. Temperature: The "Ignored" Factor at the NanoBioInterface. ACS Nano, (2013), 7 ,6555–6562.

[45] A. Nel, T. Xia, L. Madler, N. Li. Toxic potential of materials at the nanolevel. Science (2006), 311, 622-627.

[46] D. Wu, P. Yotnda. Production and detection of Reactive Oxygen Species (ROS) in cancer. Journal of Visualized Experiments (2011), 57, 3357.

[47] T. Liu, C. Wang, X. Gu, H. Gong, L. Cheng, X. Shi, L. Feng, B. Sun, Z. Liu. Drug delivery with PEGylated MoS2 nanosheets for combined photothermal and chemotherapy of cancer. Adv. Mater. (2014b), 26, 3433-3440.